Elastic anisotropy and Poisson's ratio of solid helium under pressure

A. Grechnev, S. M. Tretyak, and Yu. A. Freiman
B. Verkin Institute for Low Temperature Physics and Engineering, National Academy of Sciences, 47 Lenin Ave., 61103 Kharkiv, Ukraine

Alexander F. Goncharov
Geophysical Laboratory, Carnegie Institution of Washington, 5251 Broad Branch Road NW, Washington DC 20015, USA and Center for Energy Matter in Extreme Environments and Key Laboratory of Materials Physics, Institute of Solid State Physics, Chinese Academy of Sciences, 350 Shushanghu Road, Hefei, Anhui 230031, China

Eugene Gregoryanz
School of Physics and Centre for Science at Extreme Conditions, University of Edinburgh, Edinburgh EH9 3JZ, United Kingdom
(Received 4 May 2015; revised manuscript received 18 June 2015; published 2 July 2015)

The elastic moduli, elastic anisotropy coefficients, sound velocities and Poisson's ratio of hcp solid helium have been calculated using density functional theory in generalized gradient approximation (up to 30 TPa), and pair + triple semiempirical potentials (up to 100 GPa). Zero-point vibrations have been treated in the Debye approximation assuming ^{4}He isotope (we exclude the quantum-crystal region at very low pressures from consideration). Both methods give a reasonable agreement with the available experimental data. Our calculations predict significant elastic anisotropy of helium ($\triangle P \approx 1.14$, $\triangle S_1 \approx 1.7$, $\triangle S_2 \approx 0.93$ at low pressures). Under terapascal (TPa) pressures helium becomes more elastically isotropic. At the metallization point, there is a sharp feature in the elastic modulus C_S, which is the stiffness with respect to the isochoric change of the c/a ratio. This is connected with the previously obtained sharp minimum of the c/a ratio at the metallization point. Our calculations confirm the previously measured decrease of the Poisson's ratio with increasing pressure. This is not a quantum effect, as the same sign of the pressure effect was obtained when we disregarded zero-point vibrations. At TPa pressures, Poisson's ratio reaches the value of 0.31 at the theoretical metallization point ($V_{mol} = 0.228$ cm^3/mol, $p = 17.48$ TPa) and 0.29 at 30 TPa. For $p = 0$, we predict a Poisson's ratio of 0.38, which is in excellent agreement with the low-p-low-T experimental data.

DOI: 10.1103/PhysRevB.92.024102 PACS number(s): 67.80.B−, 62.20.de, 62.20.dj, 71.15.Mb

I. INTRODUCTION

Helium is the second element in the periodic table, as well as the second most abundant chemical element in the universe. It is a major constituent of both stars and giant planets, and it is involved in several different nuclear fusion reactions. Its high-pressure physical properties are therefore rather important for many different branches of natural science. The low-temperature behavior of helium is well-known but rather peculiar: it stays liquid up to the absolute zero while becoming superfluid, quantum freezes under pressure, and demonstrates quantum-crystal behavior in the solid phase. These quantum effects are a consequence of the relatively small mass of the He atom (≈7296 electron masses for ^{4}He) and weak interatomic interaction. Solid helium is a close-packed atomic crystal with nearly spherically symmetric He atoms. ^{4}He has hexagonal close-packed (hcp) structure everywhere except for the small body-centered cubic (bcc) and face-centered cubic (fcc) regions near the melting line on the (p,T) phase diagram [1]. The c/a ratio of the hcp structure is close to the ideal value $\sqrt{8/3} \approx 1.633$ [2,3].

While helium has been an object of intensive experimental study for more than a century, the high-pressure experimental breakthrough happened in the last few decades due to the invention of diamond anvil cells. The elastic moduli of hcp helium up to 32 GPa, as well as the sound velocities, the Poisson's ratio (PR), and the elastic anisotropy parameters, have been measured experimentally by Zha *et al.* [4]. The results were somewhat unexpected. First, a significant anisotropy of elastic properties was found. The problem of the elastic anisotropy of helium is important for high-pressure experimental techniques, as helium is frequently used as a quasi-hydrostatic medium [5]. Second, the Poisson's ratio was found to decrease with increasing pressure, which is a rather unusual behavior, as for most solids PR increases with pressure, approaching 1/2 at megabar pressures. A similar decrease of PR with pressure has been observed in solid hydrogen [6]. Such anomalous PR behavior of He was often thought to be a quantum zero-point vibration (ZPV) effect, however, as we show in the present paper and in Ref. [7], this is not the case. A theoretical calculation of elastic moduli by Nabi *et al.* [8] using density functional theory (DFT) in the local Airy gas (LAG) approximation, local density approximation (LDA), and generalized gradient approximation (GGA) soon followed the experiment. The calculated elastic moduli were in a reasonably good agreement with experiment. Unfortunately, the authors of Ref. [8] did not calculate Poisson's ratio, and did not study the elastic anisotropy in any detail either.

The goal of the present paper is to clarify the two issues introduced above. We calculate the elastic moduli of hcp He as a function of pressure using two complementary methods: DFT-GGA and semiempirical (SE) potentials, specifically focusing on the Poisson's ratio and elastic anisotropy parameters. We extend our GGA calculations into the metallic phase (up to $p = 30$ TPa) in order to check the effect of terapascal pressures and the metallization transition on the elastic properties of helium. We also study the effect of zero-point vibrations in the Debye approximation on the physical quantities in question

(for ^{4}He) in order to determine whether quantum effects play any significant role at high ($p \gtrsim 10$ GPa) pressures.

The paper is organized as follows. In Sec. II, we outline the two approaches for calculating the total energy (DFT-GGA and SE), and then give a brief introduction to the elasticity of hexagonal crystals and the algorithm of calculating elastic moduli of an hcp crystal [9], and define the physical quantities used in the present paper. In Sec. III, we present the results of our calculations.

II. METHOD

A. Total energy calculations

Helium consists of electrons and nuclei, and due to the relatively small mass of the latter, their quantum zero-point motion cannot be ignored in general. Many different numerical methods have been applied to solid helium [10–12]. The electronic subsystem can either be described from first principles, like in density functional theory (DFT)-based methods, or replaced by empirical pairwise or n-body interactions between nuclei. The quantum and thermal motion of the nuclei can be analyzed either in the harmonic approximation, or using anharmonic approaches, such as diffusion Monte Carlo (DMC) and other Monte Carlo methods [10].

For the elasticity calculations, pair potentials are not sufficient. We have opted to use DFT in the generalized gradient approximation (GGA) as our main method. We have also used pair and three-body empirical potentials for the $p \lesssim 100$ GPa range. For the quantum zero-point vibrations, we have used a simple harmonic Debye approximation (see below). While such approach is rather crude, and the use of harmonic approximations for He atoms has been recently criticized in Ref. [11], we chose it as it is computationally cheap and consistent with a full DFT treatment of the electronic subsystem.

For the density functional theory calculations, we have used the all-electron full-potential linear muffin tin orbital (FP-LMTO) code RSPt [13] with the GGA functional of Perdew, Burke, and Ernzerhof (PBE) [14]. The basis set included the $1s$, $2p$, and $3d$ electrons of helium, with two LMTO basis functions with kinetic energies -0.1 and $+0.1$ Ha per each atomic orbital, respectively. We used 847 k points in the Brillouin zone.

For the semiempirical calculations, we have used the pair and triple SE potentials described in Ref. [15]. They include the Aziz pair potential in the Silvera-Goldman form and the three-body potential in the Slater-Kirkwood form. These are exactly the potentials used in our previous works [2,3,7,16,17] on helium. The cutoff radii $R_2 = 50.2a$ and $R_3 = 10.2a$ were used for pair and triple forces, respectively, with a being the lattice constant.

Both DFT and SE calculations were performed for zero temperature, and the zero-point vibrations were neglected at first. The effect of ZPV was later accounted for in the Debye approximation. In contrast to Ref. [8], we found the pressure-dependent equilibrium c/a ratios as described in Refs. [2,3] and used them for all our calculations. All our results are well converged with respect to the number of k points (GGA) and cutoff radii (SE), respectively.

DFT-GGA and SE can be seen as complementary methods. Semiempirical potentials usually work very well for low pressures, but fail for higher pressures where four-body and higher-order n-body forces become important. For helium, the threshold pressure is of the order of 100 GPa [2,3]. GGA, on the other hand, can be inaccurate at low pressures due to the poor description of the van der Walls (vdW) forces. It has been shown [11] that the effect of the vdW forces is rather small in the gigapascal pressure range.

B. Elasticity under initial pressure

This section and the remaining part of Sec. II deal with the elasticity theory for a hexagonal crystal under pressure and the method of calculating elastic moduli numerically. It includes the main results of Refs. [9,18,19], and other works. This material has never before been gathered in one place, therefore we decided to give a brief introduction to the method as a whole, presenting all relevant formulas and stressing some important points.

If a strain is applied to an elastic medium, each point $\mathbf{r}$ of the medium is shifted to a new position $\mathbf{r}'(\mathbf{r})$, and we can define tensor u_{ij} as

$$u_{ij} \equiv \frac{\partial x_i'}{\partial x_j} = e_{ij} + \omega_{ij}, \tag{1}$$

where $e_{ij} = (u_{ij} + u_{ji})/2$ and $\omega_{ij} = (u_{ij} - u_{ji})/2$ are the symmetric strain tensor and the antisymmetric rotation tensor, respectively, and the tensor indices $i, j = 1,2,3$ number the three Cartesian (not crystal) coordinates. Summation over repeated tensor indices is assumed. In the present paper, we do not consider rotations, so we always assume that $u_{ij} = u_{ji} = e_{ij}$ and $\omega_{ij} = 0$. Note that we are not using the Lagrangian strain tensor $\eta_{ij} \equiv (u_{ij} + u_{ji} + u_{ki}u_{kj})/2$ in the present paper. The difference between e_{ij} and η_{ij} is important under external pressure.

The volume of the strained medium is

$$V' = V \det(\delta_{ij} + u_{ij}) = V + \triangle V + O(u^3), \tag{2}$$

where

$$\triangle V = V\left(u_{ii} + \tfrac{1}{2}(u_{ii})^2 - \tfrac{1}{2}u_{ij}u_{ji}\right) \tag{3}$$

is the change of volume up to the second order in u_{ij}, and we have used the identity $\det \hat{A} = \exp \mathrm{Tr} \ln\ \hat{A}$ to expand V' in powers of u_{ij}.

The elasticity theory for a medium under external stress $\sigma_{ij}^{(0)}$ is rather nontrivial [18,20] and there is no straightforward generalization of the zero-pressure stiffness tensor C_{ijkl}. However, theory simplifies for the case of the isotropic external pressure $\sigma_{ij}^{(0)} = -p\delta_{ij}$. The stress-strain relation up to the first order in u_{ij} is [18]

$$\sigma_{ij} = C_{ijkl}(p)u_{kl} - p\delta_{ij}, \tag{4}$$

where the rank-four pressure-dependent stiffness tensor $C_{ijkl}(p)$ (tensor of elastic moduli, called $\mathring{c}_{\alpha\beta\sigma\tau}$ in Ref. [18]) has the same symmetry as the zero-pressure C_{ijkl}, namely,

$$C_{ijkl} = C_{jikl} = C_{ijlk} = C_{klij}. \tag{5}$$

The elastic energy density up to the second order in u_{ij} is [18]

$$\epsilon \equiv \frac{E}{V} = \frac{1}{2}C_{ijkl}(p)u_{ij}u_{kl} - p\frac{\triangle V}{V}, \tag{6}$$

where $\triangle V$ is defined in Eq. (3). The terms of the order u^2 in $\triangle V$ are important, as they are of the same order as the first term in Eq. (6). Note that the energy density ϵ is defined with respect to the undeformed volume V, not V'. The total energy E gives the adiabatic stiffness tensor, while for the isothermic one, the Helmholtz free energy $F = E - TS$ should be used instead. In this paper, we limit ourselves to the case $T = 0$, so there is no distinction between the two. The equation of motion of the elastic medium up to the first order in u_{ij} is [18]

$$\rho\frac{\partial^2 u_i}{\partial t^2} = C_{ijkl}(p)\frac{\partial^2 u_k}{\partial x_j \partial x_l}, \tag{7}$$

where $u_i \equiv x_i' - x_i$.

When calculating the elastic moduli numerically from Eq. (6), one must be careful with the $-p\triangle V/V$ term, as it includes u^2 terms. One way of addressing the problem is to calculate bulk and shear moduli separately [9,21]. The Voigt bulk modulus is defined as the bulk modulus under the uniform *strain* (i.e., the lattice geometry is not allowed to change as the volume changes):

$$K_V = -V\left.\frac{d^2E}{dV'^2}\right|_{V'=V,\text{ fixed geometry}}. \tag{8}$$

It can be shown that $K_V(p) = C_{iikk}(p)/9$ and it does not depend on p explicitly. The Reuss bulk modulus is defined as the bulk modulus under the uniform *stress* (i.e., the lattice geometry is changed as the pressure changes):

$$K_R = -V\left.\frac{d^2E}{dV'^2}\right|_{V'=V,\text{ relaxed geom.}} = V\left(\left.\frac{dV'}{dp'}\right|_{p'=p}\right)^{-1}. \tag{9}$$

K_R is equal to $1/S_{iikk}(p)$, where $S_{ijkl}(p)$ is the compliance tensor, the inverse of $C_{ijkl}(p)$, and again it does not depend on p explicitly. The shear moduli are calculated from Eq. (6) using strains u_{ij}, which are isochoric (volume-conserving) exactly, or in the second order of u_{ij} at least, so that $\triangle V = 0$ in Eq. (6) and the elastic energy is proportional to the shear modulus in question times u^2, without any additional terms proportional to pu^2.

Hexagonal close-packed (hcp) crystal lattice has lattice vectors

$$\mathbf{a}_1 = a\begin{bmatrix}1\\0\\0\end{bmatrix}, \quad \mathbf{a}_2 = a\begin{bmatrix}-1/2\\\sqrt{3}/2\\0\end{bmatrix}, \quad \mathbf{a}_3 = c\begin{bmatrix}0\\0\\1\end{bmatrix}, \tag{10}$$

where a and c are two pressure-dependent lattice constants. The atom positions in the undeformed hcp lattice are

$$(0,0,0),\ \left(\tfrac{2}{3},\tfrac{1}{3},\tfrac{1}{2}\right) \tag{11}$$

in crystal coordinates. When a uniform strain u_{ij} is applied to the medium, any point x_i changes to $x_i' = (\delta_{ij} + u_{ij})x_j$, i.e., the atoms form a deformed crystal lattice with new lattice vectors

$$a_i' = (\delta_{ij} + u_{ij})a_j. \tag{12}$$

Special care must be taken when applying strain to a lattice with more than one atom per unit cell. The expression (12) determines only the change of three lattice vectors under strain, but tells nothing about the positions of the atoms within the unit cell. Such positions are not determined by macroscopic elasticity theory and must be allowed to relax in total energy calculations. If they change linearly in u_{ij} under strain, this affects the calculated elastic constants. In other words, to obtain correct results, we must minimize the total energy with respect to all atomic positions for each applied finite strain. The hcp lattice has two atoms per unit cell, and their positions are fixed by symmetry for the undeformed lattice, however, for certain strains (like the orthorhombic strain, see below), they indeed change linearly in u_{ij}.

In Voigt notation,

$$(11,22,33,23,31,12) \to (1,2,3,4,5,6), \tag{13}$$

the stiffness tensor of a hexagonal crystal is specified by five independent elastic constants C_{11}, C_{12}, C_{13}, C_{33}, and C_{44}:

$$C_{ij} = \begin{bmatrix} C_{11} & C_{12} & C_{13} & 0 & 0 & 0 \\ C_{12} & C_{11} & C_{13} & 0 & 0 & 0 \\ C_{13} & C_{13} & C_{33} & 0 & 0 & 0 \\ 0 & 0 & 0 & C_{44} & 0 & 0 \\ 0 & 0 & 0 & 0 & C_{44} & 0 \\ 0 & 0 & 0 & 0 & 0 & \frac{1}{2}(C_{11} - C_{12}) \end{bmatrix}. \tag{14}$$

C. Calculation of elastic constants

If we have any method of calculating the energy of the crystal for a given volume V, c/a ratio, and strain u_{ij}, like DFT or SE, we can calculate the five elastic constants numerically by applying the several independent strains in Eq. (6). An efficient way to do this for the hcp lattice has been proposed by Steinle-Neumann *et al.* [9]. As explained above, bulk and shear moduli are calculated separately.

First, we calculate the total energy $E(V)$ as a function of volume (in practice, the molar volume $V_{\text{mol}} = VN_A/N$ is used, where N is the number of atoms, and N_A is Avogadro's number). For each volume, the energy minimum with respect to the ratio c/a is found, and $E(V)$ is defined as the energy of this minimum. The ideal c/a ratio (corresponding to the close-packing of hard spheres) is $\sqrt{8/3} \approx 1.633$, and for helium the c/a ratio is rather close to the ideal value [2]. The equation of state (EOS) $p(V)$ and the Reuss bulk modulus K_R are found as

$$p = -\frac{dE}{dV}, \quad K_R = -V\frac{dp}{dV} = \frac{d^2E}{dV^2}. \tag{15}$$

In practice, the energy $E(V)$ is approximated (via least square fit) by the Rose-Vinet equation of state [22], which allows for an accurate numerical differentiation. For GGA, we were unable to find a single Rose-Vinet fit, which would be accurate in both GPa and TPa pressure ranges, therefore we had to use two different parametrizations.

By using a diagonal stress $\sigma_{ij} = -(p + \triangle p)\delta_{ij}$, which is an infinitesimal change of pressure, we can show that the Reuss bulk modulus is

$$K_R = \frac{Q}{C_S}, \tag{16}$$

where

$$Q \equiv C_{33}(C_{11}+C_{12}) - 2C_{13}^2, \tag{17}$$

$$C_S \equiv C_{11}+C_{12}+2C_{33}-4C_{13}. \tag{18}$$

The corresponding strain [found from Eq. (4)] is

$$u_{ij} = -\frac{\triangle p}{Q}\begin{bmatrix} C_{33}-C_{13} & 0 & 0 \\ 0 & C_{33}-C_{13} & 0 \\ 0 & 0 & C_{11}+C_{12}-2C_{13} \end{bmatrix}. \tag{19}$$

Equation (16) is the first equation we use for determining five elastic constants. From Eq. (19), we can find the logarithmic derivative of c/a with respect to volume

$$R \equiv -\frac{d\ln(c/a)}{d\ln V} = \frac{1}{C_S}(C_{33}+C_{13}-C_{11}-C_{12}). \tag{20}$$

This is the second equation we need. An analytic parametrization of $c/a(V_{\rm mol})$ is used for numerical differentiation as usual.

From now on we are going to use only exactly isochoric (volume-conserving) strains as explained above. In order to calculate C_S, Ref. [9] used an isochoric c/a-changing strain, however, it is not necessary, as we can use an equivalent formula,

$$C_S = \frac{9}{2V}\left(\frac{c}{a}\right)^2 \frac{\partial^2 E(V,c/a)}{\partial(c/a)^2}, \tag{21}$$

taken at the equilibrium c/a. We use the energies $E(V,c/a)$ calculated previously when we looked for the equilibrium c/a for each volume and approximate it by a fourth-order polynomial of c/a. Equation (18) with C_S from Eq. (21) is the third equation for the five elastic moduli. We now have three equations for three variables, $C_{11}+C_{12}$ (in this combination only), C_{13}, and C_{33}. They can be solved to obtain

$$C_{11}+C_{12} = 2K_R + \frac{C_S}{9}(2R-1)^2, \tag{22}$$

$$C_{13} = K_R + \frac{C_S}{9}(2R-1)(R+1), \tag{23}$$

$$C_{33} = K_R + \frac{2C_S}{9}(R+1)^2. \tag{24}$$

We need two more isochoric strains to find C_{44} and $C_{66} \equiv (C_{11}-C_{12})/2$. C_{44} is found from the monoclinic strain

$$u_{ij} = \begin{bmatrix} 0 & 0 & t \\ 0 & \frac{t^2}{1-t^2} & 0 \\ t & 0 & 0 \end{bmatrix}, \tag{25}$$

with $\epsilon = 2C_{44}t^2 + O(t^4)$. Alternatively, C_{44} for the hcp lattice can be obtained from the calculated E_{2g} Raman frequency using the formula [23]

$$C_{44} = \frac{m}{4\sqrt{3}}\frac{c}{a^2}\nu_{E_{2g}}^2, \tag{26}$$

as we did previously in Ref. [17]. The resulting values for C_{44}, obtained using these two approaches agree within 1%. For C_{66}, we use the orthorhombic strain

$$u_{ij} = \begin{bmatrix} t & 0 & 0 \\ 0 & -t & 0 \\ 0 & 0 & \frac{t^2}{1-t^2} \end{bmatrix}, \tag{27}$$

which gives $\epsilon = 2C_{66}t^2 + O(t^4) = (C_{11}-C_{12})t^2 + O(t^4)$. Note that for this strain the atomic positions change under strain. The position of atom 2, which is (2/3,1/3,1/2) for the undeformed lattice, becomes $((1+\lambda)/2,\lambda,1/2)$, with the parameter λ depending linearly on t as $\lambda = 1/3 - gt + O(t^2)$. It means that we have to relax the parameter λ for each finite strain t in order to calculate the correct elastic energy. In our calculations of C_{44} and C_{66}, we have used five t points $t = 0, \pm 0.005, \pm 0.010$ (for very high pressures smaller values of t were used) and interpolated the energy $E(t)$ with a fourth-order polynomial in order to find the coefficient before t^2. The results obtained this way are virtually independent on the particular values of t used. Such approach is vital for C_{66}, while for C_{44} the $E(t)$ dependence is almost exactly quadratic in t in a wide range of t. With C_{44} and C_{66} calculated, we can finally determine all five elastic constants of the hcp lattice. The quantities C_{44}, C_{66}, and $C_S/6$ are three different shear moduli for three independent pure shear (isochoric) deformations. They are all equal for an isotropic solid.

D. Anisotropy parameters

The three acoustic sound velocities (one compressional and two shear ones) of the hexagonal lattice are [6,24]

$$\rho v_P^2 = \frac{A+B}{2}, \tag{28}$$

$$\rho v_{S1}^2 = \frac{C_{11}-C_{12}}{2}\sin^2\theta + C_{44}\cos^2\theta, \tag{29}$$

$$\rho v_{S2}^2 = \frac{A-B}{2}, \tag{30}$$

where

$$A \equiv C_{11}\sin^2\theta + C_{33}\cos^2\theta + C_{44}, \tag{31}$$

$$B^2 \equiv [(C_{11}-C_{44})\sin^2\theta + (C_{44}-C_{33})\cos^2\theta]^2 + (C_{13}+C_{44})^2\sin^2(2\theta), \tag{32}$$

and θ is the angle between the wave vector **q** and **z**.

The elastic anisotropy of a hexagonal crystal can be described by the anisotropy parameters of these three acoustic waves [9]:

$$\triangle P = \frac{C_{33}}{C_{11}}, \tag{33}$$

$$\triangle S_1 = \frac{C_{11}+C_{33}-2C_{13}}{4C_{44}} = \frac{C_S+2C_{66}}{8C_{44}}, \tag{34}$$

$$\triangle S_2 = \frac{2C_{44}}{C_{11}-C_{12}} = \frac{C_{44}}{C_{66}}. \tag{35}$$

For an isotropic medium, this quantities are equal to one. Note that for a cubic crystal, $\triangle P$ is equal to unity, and $\triangle S_1$ is the single anisotropy parameter $(C_{11}-C_{12})/(2C_{44})$ of the cubic crystal. $\triangle S_2$ is ambiguous, as there is no condition $C_{66} = (C_{11}-C_{12})/2$ for the cubic symmetry, but instead $C_{44} = C_{66}$.

E. Aggregate properties: Voigt and Reuss approaches

Aggregate description replaces an actual crystal with an effective isotropic elastic medium, described by an average bulk modulus K and an average shear modulus G, with

$$C_{ijkl} = \left(K - \tfrac{2}{3}G\right)\delta_{ij}\delta_{kl} + G(\delta_{ik}\delta_{jl} + \delta_{il}\delta_{jk}). \quad (36)$$

It is a good approximation for polycrystalline solids and mixtures. The compressional and shear sound velocities are

$$v_P = \left(\frac{K + \frac{4}{3}G}{\rho}\right)^{\frac{1}{2}}, \quad v_S = \left(\frac{G}{\rho}\right)^{\frac{1}{2}}. \quad (37)$$

This is often written as $v_P^2 = v_B^2 + \frac{4}{3}v_S^2$ with $v_B = (K/\rho)^{\frac{1}{2}}$ being the bulk (hydrodynamic) sound velocity. It has no direct physical meaning for a crystal, however, it corresponds to the sound velocity of the liquid phase, as can be seen at the liquid-solid transition in Ref. [4]. The Poisson's ratio is defined as

$$\sigma \equiv \frac{1}{2}\frac{3K - 2G}{3K + G} = \frac{1}{2}\frac{3v_B^2 - 2v_S^2}{3v_B^2 + v_S^2} = \frac{1}{2}\frac{v_P^2 - 2v_S^2}{v_P^2 - v_S^2}. \quad (38)$$

In order to find the values of K and G consider a polycrystalline solid consisting of grains of all possible orientation, and use Voigt and Reuss estimates of its elastic moduli. In the Voigt approach, a uniform *strain* field u_{ij} (of either uniform compression or a shear type) is applied to the mixture, and K and G are found from the averaged elastic energy density. For a polycrystal, this means averaging the elastic energy over all possible orientations of the crystal relative to the strain field u_{ij}. The Reuss approach uses uniform *stress* instead. The bulk moduli defined in this way are equal to K_V and K_R defined above. For a hexagonal lattice, the bulk and shear moduli are [19]

$$K_V = \tfrac{1}{9}(2C_{11} + C_{33} + 2C_{12} + 4C_{13}),\ K_R = \frac{Q}{C_S}, \quad (39)$$

$$G_V = \tfrac{1}{30}(C_S + 12C_{44} + 12C_{66}), \quad (40)$$

$$G_R = \frac{5}{2}\frac{QC_{44}C_{66}}{3K_VC_{44}C_{66} + Q(C_{44} + C_{66})}. \quad (41)$$

Finally, we use the Voigt-Reuss-Hill average scheme to obtain K and G:

$$K = \frac{K_V + K_R}{2}, \quad G = \frac{G_V + G_R}{2}. \quad (42)$$

F. Zero-point vibrations

In our calculations, we have treated zero-point vibrations within the framework of the Debye model. As discussed above, this approach is by no means exact, especially at low pressures, but it gives us a good estimate of the effect of ZPV on the elastic properties. Using K and v_S obtained in the absence of ZPV, we calculate the Debye temperature

$$T_D = \frac{\hbar}{k_B}\left[\frac{V_{\rm mol}}{18\pi^2 N_A}\left(\frac{1}{v_P^3} + \frac{2}{v_S^3}\right)\right]^{-1/3}, \quad (43)$$

zero-point energy

$$E_{zp} = \frac{9}{8}Nk_BT_D, \quad (44)$$

and the corresponding contributions to pressure and the bulk modulus:

$$\triangle p = -\frac{dE_{zp}}{dV} = -\frac{9}{8}N_Ak_B\frac{dT_D}{dV_{\rm mol}}, \quad (45)$$

$$\triangle K = -V_{\rm mol}\frac{d\triangle p}{dV_{\rm mol}} = \frac{9}{8}V_{\rm mol}N_Ak_B\frac{d^2T_D}{dV_{\rm mol}^2}. \quad (46)$$

We find the volume derivatives of T_D analytically, using the Rose-Vinet expression for K and a simple parametrization for v_S. Below, we always compare results with and without ZPV in order to measure the importance of quantum effects on each physical quantity. ^{4}He isotope was assumed for all our ZPV calculations.

III. RESULTS AND DISCUSSION

A. Equation of state, metallization, and the c/a ratio

The calculated equations of state (EOS) $p(V_{\rm mol})$ of the hcp helium are presented in Fig. 1 and compared with the experimental data [4]. The four curves correspond to our four approaches: SE and GGA, with and without ZPV. EOS can be viewed as an auxiliary quantity in our calculations, as it is used to calculate the Reuss bulk modulus. It is also used to change variables from $V_{\rm mol}$ to p, which is done to obtain the p-dependent quantities presented in all figures of the present paper. For this, we always used the respective EOS for each of the four approaches, e.g., a GGA + ZPV EOS was used for GGA + ZPV elastic moduli, but SE (No ZPV) EOS was used for SE (No ZPV) elastic moduli.

The semiempirical potentials underestimate the pressure p for a given $V_{\rm mol}$, but zero-point vibrations improve the agreement with the experiment significantly. GGA overestimates the pressure, and the inclusion of ZPV makes things worse.

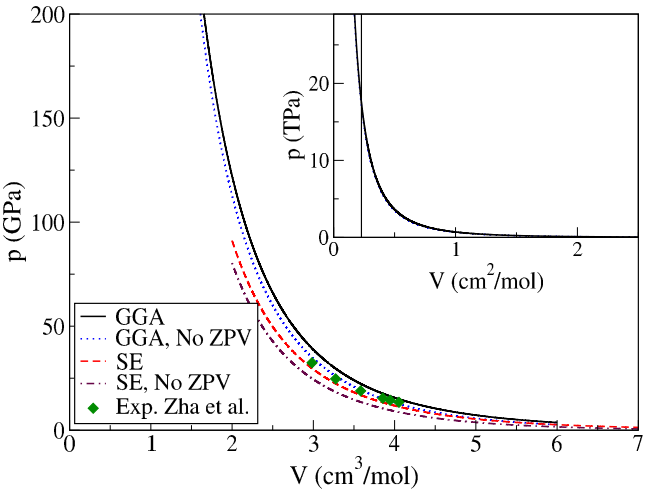

FIG. 1. (Color online) Equation of state of hcp helium. (Inset) High-pressure region. The vertical line indicates the GGA metallization point.

The effect of ZPV is more pronounced in the SE approach, as the SE pressure for a given V_{mol} is smaller compared to GGA.

The inset of Fig. 1 shows the high-pressure EOS (GGA with and without ZPV) for pressures up to the metallization point and above. The metallization takes place at $V_{\mathrm{mol}} = 0.228$ cm^3/mol in our GGA calculations [3] ($p = 17.48$ TPa from our GGA + ZPV EOS, or $p = 17.08$ TPa without ZPV). This point is shown as the vertical line in the inset of Fig. 1. Our metallization volume and pressure are in good agreement with previous GGA results [12,25]. Note, however, that GGA seriously overestimates the metallization volume (by about 20% for He according to the diffusion Monte Carlo and GW studies [12,25]), thus underestimating the metallization pressure. Moreover, it has been recently shown [12] that vibrational degrees of freedom further increase the metallization pressure, but these effect cannot be reproduced in the harmonic approximation. Reference [12] gives the value $p = 32.9$ TPa. Such questions are beyond the scope of the present paper. We use only GGA with ZPV in the harmonic Debye approximation, which results in an underestimated metallization pressure of 17.48 TPa.

Our calculated c/a ratios have been presented previously in Refs. [2,3]. SE and GGA give somewhat different $c/a(V_{\mathrm{mol}})$ curves, but both methods give lattice distortions $\delta \equiv c/a - \sqrt{8/3}$ of the order of 10^{-3} at pressures up to 150 GPa. δ is negative for $p > 13$ GPa in both approaches. For the TPa pressures, the magnitude of the negative δ obtained with GGA grows, and it reaches a sharp minimum $\delta \approx -0.05$ at the metallization point $V_{\mathrm{mol}} = 0.228$ cm^3/mol (Ref. [3]).

B. Elastic moduli and the elastic anisotropy

The five elastic moduli for the pressures up to 150 GPa are presented in Fig. 2. Again, we compare our four theoretical approaches with the experimental data of Zha *et al.* [4]. Note that all our calculations were done for $T = 0$, while the experimental elastic moduli were measured at room temperature $T = 300$ K, which can be one of the reasons for the theory-experiment discrepancies. Both SE and GGA are in reasonable agreement with the experiment, although neither method gives a perfect quantitative match. GGA seems to be the more consistent of the two. Our GGA results without ZPV are close to the GGA and LAG results obtained in Ref. [8]. The DFT-GGA errors mainly stem from the inaccuracy of the GGA functional itself, we have checked that the parameters of the FP-LMTO calculations (number of k points, tail energies, etc.) have minimal effect on the results. It is unlikely that the errors of the SE approach (at least for the pressures $p \lesssim 50$ GPa) are caused solely by the neglect of the four-body and higher-order n-body forces. The most likely reason for the SE-experiment differences (apart from the temperature effect) is that the elastic moduli are sensitive to the particular parametrization [15] of the pair and triple forces. The effect of ZPV, while noticeable, does not affect the elastic moduli in any drastic way.

In Fig. 3, the calculated elastic moduli (GGA + ZPV) are presented for the terapascal pressure range. The two additional shear moduli C_{66} and $C_S/6$ are also shown. Significant features are seen at the GGA metallization point $p = 17.48$ TPa. They are most likely finite discontinuities (steps), however, the critical behavior at the metallization transition is beyond the scope of the present paper and would be difficult to investigate accurately with the methods we employ. Of the

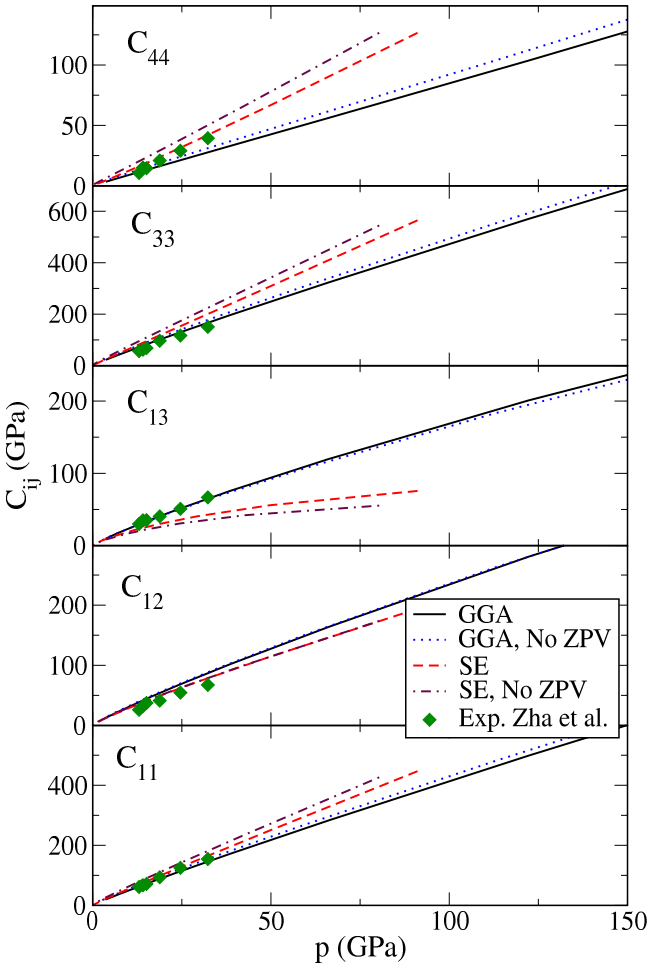

FIG. 2. (Color online) Five elastic constants of hcp helium vs pressure.

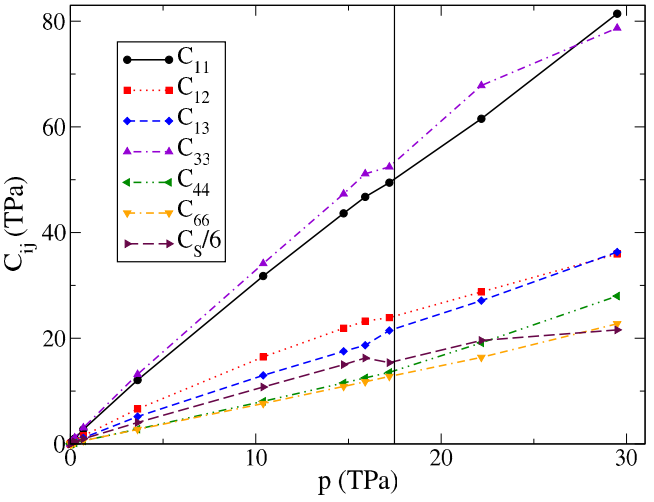

FIG. 3. (Color online) Elastic moduli (GGA + ZPV only) of hcp helium under terapascal pressures. Symbols are the calculated data points. The vertical line indicates the GGA metallization point. $C_{66} \equiv (C_{11} - C_{12})/2$ and $C_S/6$ are also presented.

three elemental shear moduli only $C_S/6$ has a large jump ($\approx -5\%$) at the metallization point, while the behavior of C_{44} and C_{66} is relatively smooth. Remember that C_S is the measure of stiffness of the crystal with respect to the isochoric change of the c/a ratio, so it is not unexpected that the behavior of C_S is irregular at the point where c/a has a sharp minimum [3]. Note that $C_S(p)$ also behaves rather nonlinearly in the metallic phase. These irregularities in C_S affect the five elastic constants, most notably C_{13} and C_{33}, via Eqs. (22)–(24). The hcp lattice is dynamically stable for the whole pressure range considered, i.e., the conditions [8] $C_{44} > 0$, $C_{11} > |C_{12}|$, $C_{11}C_{33} > (C_{13})^2$ and $C_{33}(C_{11} + C_{12}) > 2C_{13}^2$ are fulfilled, which ensures that the single-crystal sound velocities (28)–(30) are real.

All our calculations were done for the relaxed c/a ratio, and the effect of the volume dependence of c/a has been taken into account through the parameter R. In order to test the importance of the c/a distortion for the elastic moduli, we have also performed calculations with $R = 0$, like in Ref. [8]. Our results (not shown) indicate that the difference is barely visible for pressures up to 150 GPa, however, it becomes significant (about 5%) for the TPa pressure range, and it noticeably affects the features near the metallization point. We took great care in choosing the parametrization of the function $c/a(V_{\rm mol})$ that reproduces the sharp minimum in c/a well.

The elastic anisotropies $\triangle P$, $\triangle S_1$, and $\triangle S_2$ are presented in Fig. 4. The compressional anisotropy $\triangle P$ is close to the isotropic value of 1 in the experiment, however, both GGA and SE predict a noticeable anisotropy $\triangle P > 1$. GGA gives a virtually pressure independent value $\triangle P \approx 1.14$, while the semiempirical $\triangle P$ grows from $\approx$1.1 at low pressures to $\approx$1.25 at 100 GPa. $\triangle S_1$ is about 1.2–1.3 in the experiment, both GGA and SE overestimate it significantly, giving values of the order of 1.6–1.7. The third parameter, $\triangle S_2$, is always less than one in both theory and experiment. SE and GGA, however, give values closer to 1 than the experiment, thus underestimating the anisotropy.

To summarize, GGA gives $\triangle P \approx 1.14$, $\triangle S_1 \approx 1.7$, $\triangle S_2 \approx 0.93$ and the pressure dependencies of these parameters are rather small. The SE approach, while agrees well with GGA for low pressures, predicts a much stronger pressure dependence of $\triangle P$ and $\triangle S_{1,2}$ and a different sign for $d\triangle S_1/dp$. Reference [8] states that the three anisotropy parameters are nearly pressure-independent. While our GGA data fully confirm this result, our SE data behave quite differently. In the absence of reliable experimental data on the pressure dependencies, it is hard to say which behavior is more correct (see the discussion below, however). Both methods overestimate $\triangle P$ and $\triangle S_1$ significantly, and also overestimate $\triangle S_2$ (which underestimates the anisotropy), thus neither approach agrees particularly well with the experiment. In particular, the relative errors in $\triangle P$, $\triangle S_1$, and $\triangle S_2$ (computed relative to the experiment) are significantly larger than the errors in C_{ij}. The reasons for such discrepancy are unknown. Since both GGA and SE agree with each other better than with the experiment, one can speculate that the difference in temperature between 0 and 300 K might play at least some role. The large elastic anisotropy of He, while somewhat unexpected, is not in any way incompatible with the high symmetry of the hcp crystal and the nearly spherical shape of the atoms.

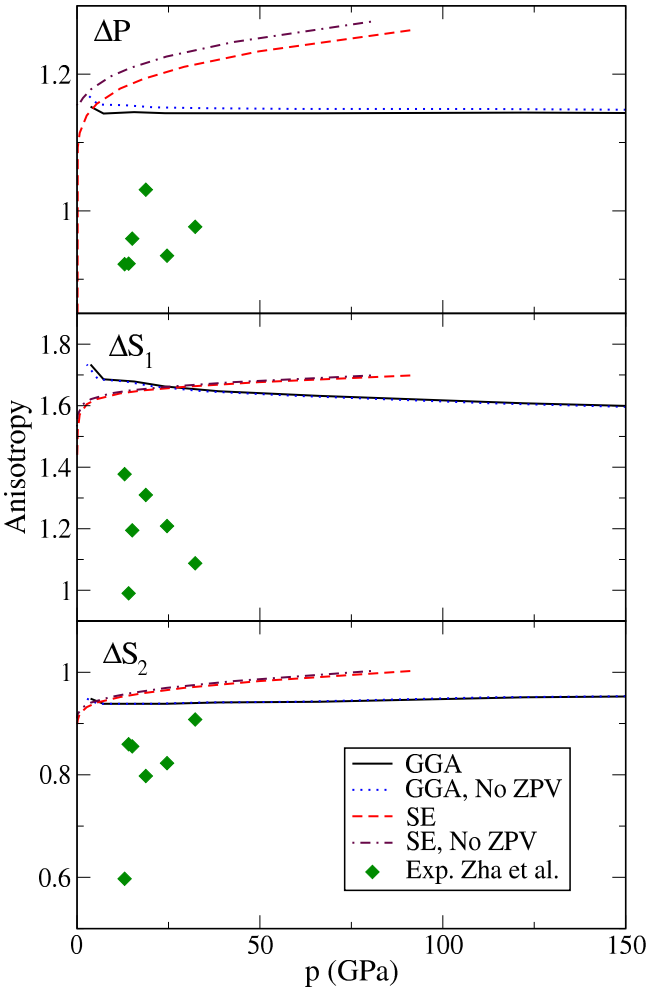

FIG. 4. (Color online) Elastic anisotropy parameters of hcp helium vs pressure.

Highly-symmetric crystals have isotropic or nearly isotropic rank-2 tensor properties, such as conductivity, thermal expansion, or dielectric permittivity. The stiffness, however, is a rank-4 tensor property, and it is well-known that even cubic crystals are not elastically isotropic. The large values of $\triangle S_1$ are not very surprising, since this parameter is similar to the single anisotropy parameter $(C_{11} - C_{12})/(2C_{44})$ of the cubic crystal.

The three anisotropy parameters at TPa pressures are presented in Fig. 5, upper panel. In the insulator phase, anisotropy decreases with pressure, with three parameters becoming close to unity just before the metallization transition. This is an intuitively plausible behavior of the atomic crystal becoming more isotropic under pressure. However, $\triangle P$, $\triangle S_1$, and $\triangle S_2$ demonstrate strong features at the metallization point (especially $\triangle S_1$, which involves C_S), with the anisotropies of the two shear modes changing sign at the metallization transition, and $\triangle P$ staying close to one and showing nonlinear behavior in the metallic phase. One can understand the anisotropy parameters in terms of the elastic moduli presented in Fig. 3. For instance, let us analyze $\triangle S_1$. For an isotropic solid, $C_{44} = C_{66} = C_S/6$. For helium at low pressures, however, $C_S/6$ has almost twice the value of C_{44},

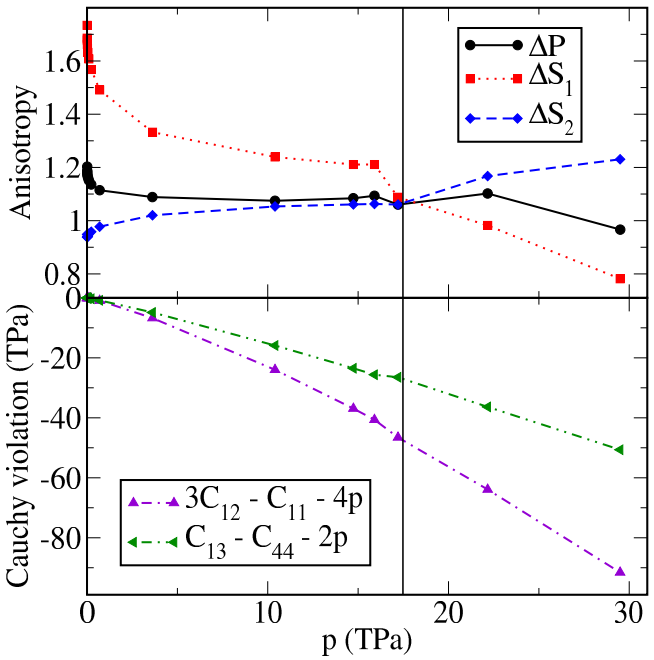

FIG. 5. (Color online) Elastic anisotropy parameters (top) and Cauchy violations (bottom) of hcp helium under terapascal pressures. Symbols are the calculated data points. The vertical line indicates the GGA metallization point.

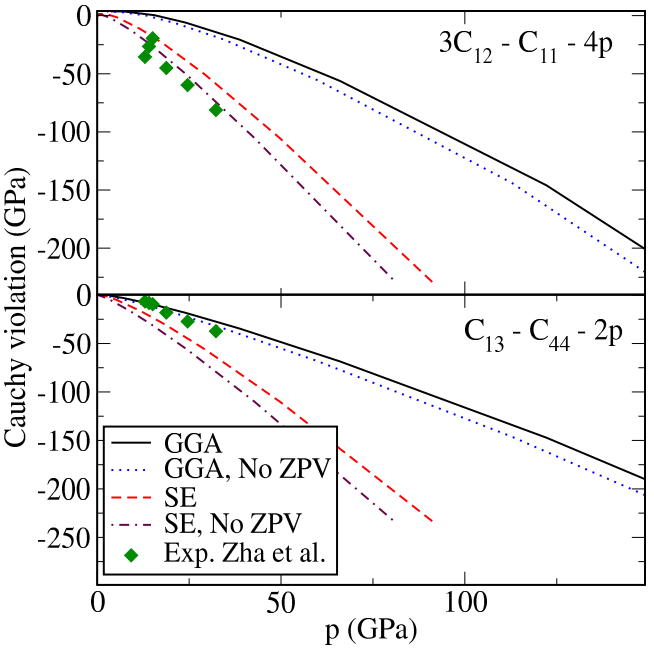

FIG. 6. (Color online) Cauchy violations of hcp helium vs pressure.

giving a large $\triangle S_1$. At higher pressures, $C_S/6$ is of the same order as C_{44} and C_{66}, and eventually becomes smaller than them in the metallic phase, which corresponds to $\triangle S_1 < 1$.

Strictly speaking, it is wrong to say that the anisotropy parameters are nearly pressure-independent. Indeed, the pressure-induced changes in Fig. 5 are rather dramatic even if we consider the insulating phase only. The pressure independence found in Fig. 4, and in Ref. [8], is simply the result of the pressure scale of 150 GPa being very small compared to the metallization pressure ∼17 TPa, which is presumably the only natural pressure scale in solid helium (if the quantum effects are disregarded). From this logic, we can infer that GGA is more trustworthy than SE in determining the pressure dependence of $\triangle P$ and $\triangle S_{1,2}$, since it gives reasonable results in the TPa range of pressures, while the SE method breaks down at $p \sim 100$ GPa, which can act as a spurious pressure scale. This argument is far from infallible, however, as GGA is known to be unreliable for pressures $p \lesssim 50$ GPa due to the poor description of the van der Walls forces.

The Cauchy violations $3C_{12}-C_{11}-4p$ and $C_{13}-C_{44}-2p$ are presented in Fig. 6. They can be thought of as a measure of noncentral forces in a solid. Experimental $3C_{12}-C_{11}-4p$ is reproduced well by SE and not so well by GGA, but the situation is reversed for $C_{13}-C_{44}-2p$. The Cauchy violations at terapascal pressures are shown in Fig. 5, lower panel. Their behavior is mostly linear with mild kinks at the metallization point.

C. Aggregate properties

The Voigt-Reuss-Hill-averaged bulk and shear moduli are presented in Fig. 7. For the bulk modulus K, both methods agree very well with the experiment and the difference between GGA and SE is small. For the shear modulus G, however, there is a significant difference between GGA and SE. Figure 8 shows the three sound velocities v_P, v_B, and v_S. Both GGA and SE agree with the experiment pretty well, with v_S (which is proportional to $\sqrt{G}$) displaying the largest SE-GGA difference. We also plot $\sqrt{C_{44}/\rho}$ (calculated with GGA + ZPV) as the golden dash-dot-dot curve in the lower panel of Fig. 8. It has a meaning of v_S calculated by using the modulus C_{44} instead of the averaged shear modulus G, like we did previously in Ref. [17]. For an isotropic solid, $G = C_{44}$. For helium, using C_{44} instead of G underestimates v_S by a few percent and worsens the agreement between GGA and the experiment. In other words, by calculating v_S from the proper Voigt-Reuss-Hill G in the present work we actually improve the GGA-experiment agreement compared to Ref. [17].

The bulk and shear moduli and sound velocities at TPa pressures are presented in Fig. 9. All these quantities show features at the metallization point, with kinks in G and, respectively, v_S, being the most pronounced.

The Debye temperature T_D is presented in Fig. 7, lower panel. Just like with shear modulus G, there is a significant difference between SE and GGA, with experimental data points lying in the middle. The Debye temperature for the TPa pressures is plotted in Fig. 10, upper panel. It shows a noticeable feature at the metallization point.

D. Poisson's ratio

Figure 11 shows the Poisson's ratio σ as a function of pressure. The GGA + ZPV results [7], obtained using C_{44} instead of G, as explained above, are also plotted as the golden dash-dot-dot curve. In addition to the experimental data of Zha *et al.* [4], we also plot the low-p, low-T data of Nieto *et al.* [26]. Since the Poisson's ratio (38) is proportional to the

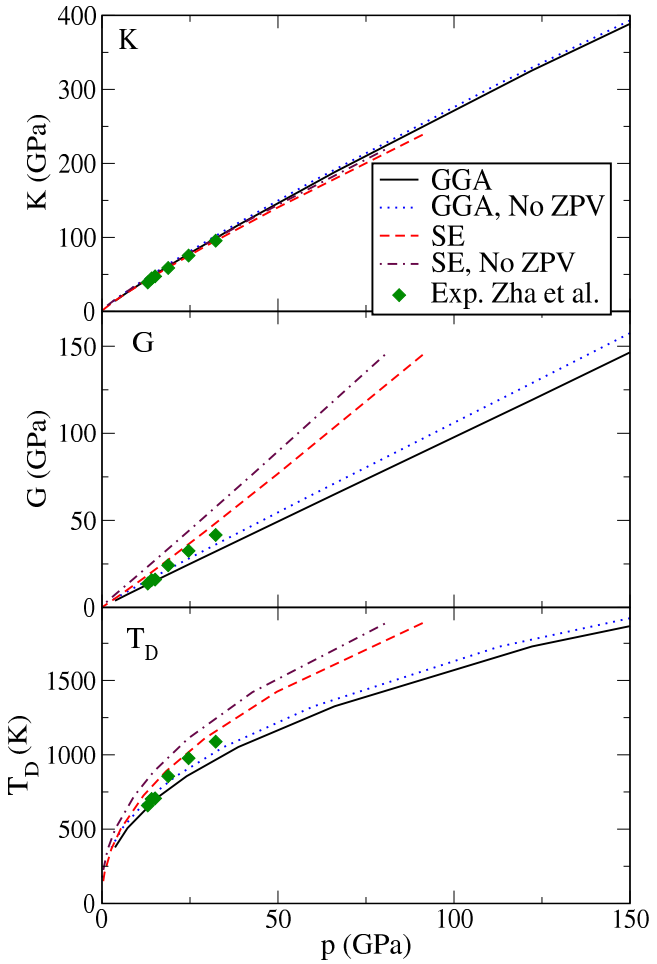

FIG. 7. (Color online) Aggregate properties of hcp helium vs pressure: bulk modulus K (top), shear modulus G (middle), and Debye temperature (bottom). K and G are obtained using the Voigt-Reuss-Hill averaging.

difference $3K - 2G$, it is a rather method-sensitive quantity. Just like for the elastic anisotropy parameters above, SE gives a much stronger pressure dependence of σ compared to GGA, and for the reasons outlined above for $\triangle P$ and $\triangle S_{1,2}$ we find GGA results more trustworthy in this aspect. On the other hand, the experimental pressure dependence of σ seems to be closer to the SE one. Neither method agrees perfectly with the $T = 300$ K experimental data of Zha *et al.* [4], however, *both* our methods agree *quantitatively* with the $p \approx 0, T \approx 0$ result of Nieto *et al.* [26] ($\sigma = 0.38$, the purple dot in Fig. 11) as long as ZPV is included.

Although different theoretical and experimental methods give somewhat different values of σ, they all agree upon one fact: $d\sigma/dp < 0$, i.e., σ decreases monotonously when pressure increases, fully confirming the surprising result of Zha *et al.* In particular, while the role of ZPV for σ is somewhat larger than for other quantities studied in the present paper, and σ shows an isotopic effect [26], the negative pressure dependence of σ is definitely not a quantum effect, as the "No ZPV" curves show the same sign and order of magnitude of $d\sigma/dp$. This behavior of σ is highly unusual, although solid hydrogen [6,7] also has negative $d\sigma/dp$ at least for low

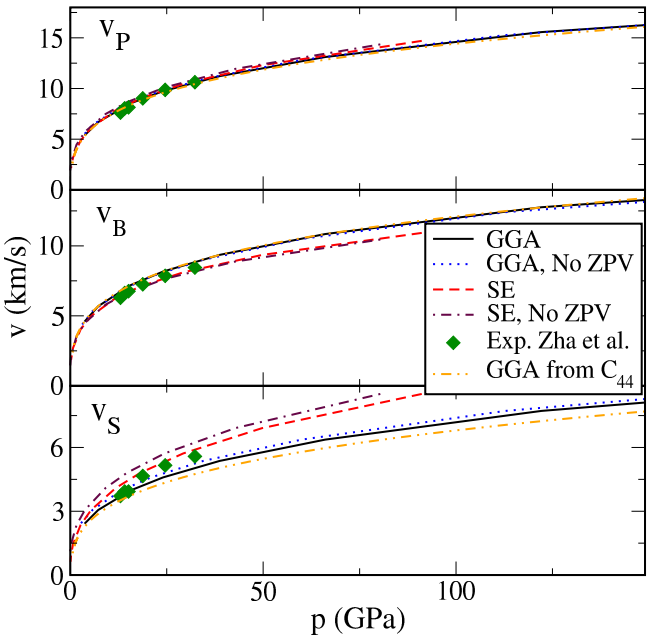

FIG. 8. (Color online) Aggregate sound velocities of hcp helium vs pressure.

pressures. All heavier rare-gas solids (RGSs) [7] have positive $d\sigma/dp$. The difference in behavior between He and heavier RGSs is, we repeat, not a quantum effect, i.e., it is not caused by the small mass of He atoms. Presumably, the crucial factor here is the difference of the outermost electron shells in He ($1s^2$ shell) and heavier RGSs (ns^2np^6). The situation is similar

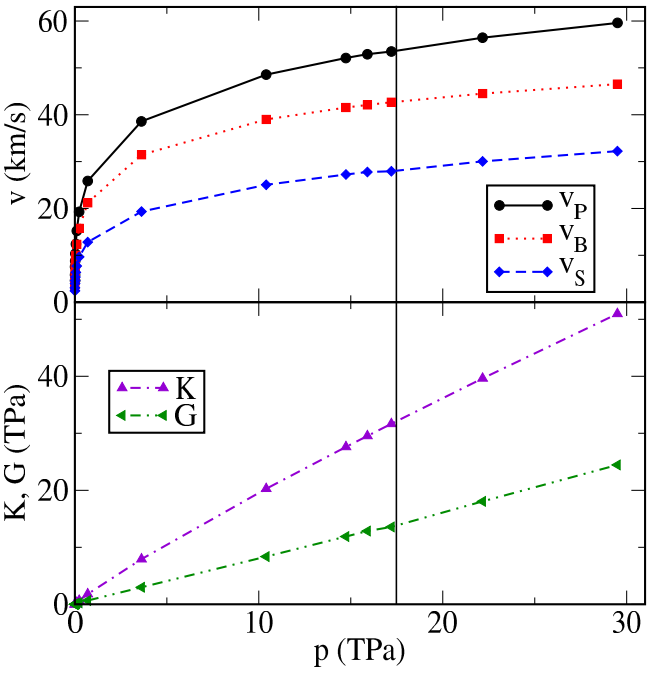

FIG. 9. (Color online) Aggregate properties of hcp helium in the TPa-pressure range: sound velocities (top), bulk, and shear moduli (bottom). Symbols are the calculated data points. The vertical line indicates the GGA metallization point.

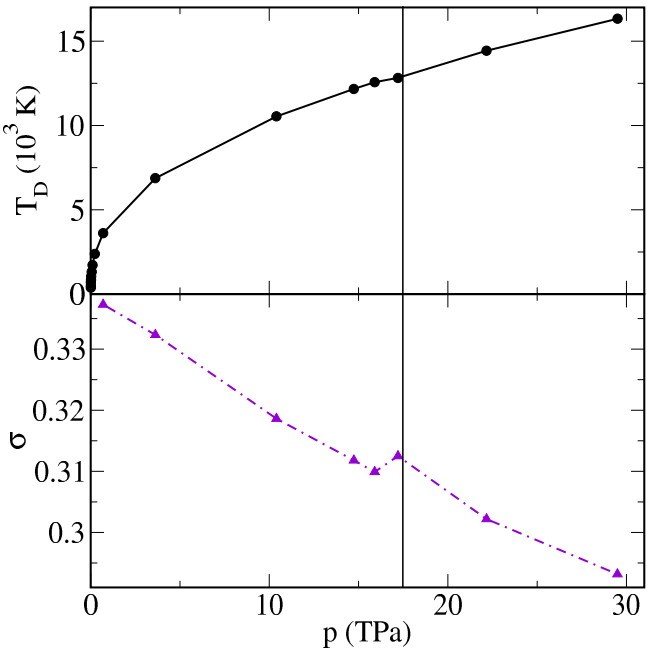

FIG. 10. (Color online) Debye temperature (upper panel) and Poisson's ratio (bottom) of hcp helium in the terapascal-pressure range. Symbols are the calculated data points. The vertical line indicates the GGA metallization point.

for $c/a - \sqrt{8/3}$, which have different sign for He and other RGS's in GGA [3]. In the language of SE potential, both types of behavior of σ can be accounted for by using pair and triple forces of exactly the same functional form [15], but with different values of parameters.

The Poisson's ratio at terapascal pressures is plotted in Fig. 10, lower panel. σ decreases monotonously up to highest pressures apart from a large feature at the metallization point. There is no minimum in σ (disregarding the step at the metallization point) and definitely no $\sigma \to 0.5$ high-pressure

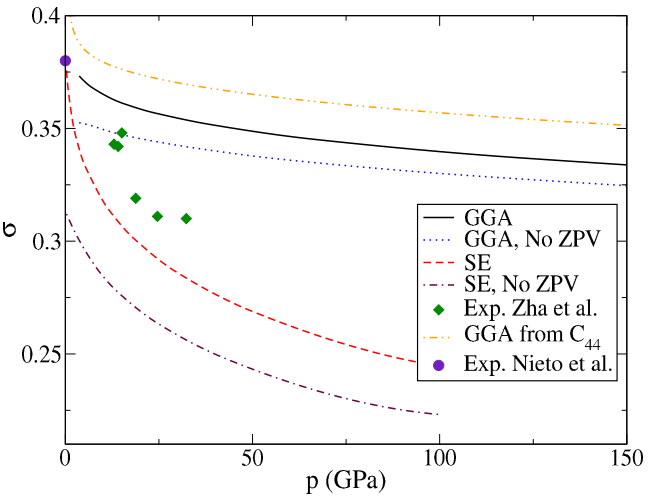

FIG. 11. (Color online) Poisson's ratio of hcp helium vs pressure.

asymptotic that many materials have. At the highest pressures considered σ is of the order of 0.29.

A question often asked is whether helium becomes a classical crystal under high pressure, or in other words, whether the relative effect of ZPV on various physical quantities decreases with pressure. This question is surprisingly nontrivial, as it depends on the complicated interplay of the kinetic and potential energy of the He atoms. A recent diffusion Monte Carlo analysis [11] has shown that the kinetic to potential energy ratio $|E_{\rm kin}/E_{\rm pot}|$ (which can be viewed as the measure of quantumness) does indeed decrease monotonously with pressure, however, this decrease becomes very slow for pressures $p \gtrsim 85$ GPa. We have reached similar conclusions in the present work, which is best seen for Poisson's ratio (Fig. 11). σ is dimensionless, and the difference between classical and quantum σ slowly decreases with pressure. In particular, this difference is of the order of 0.01 in the 150-GPa pressure range, but in the TPa range (not shown) it reaches the value of about 0.0035.

IV. CONCLUSION

We have calculated five elastic constants of hcp helium under pressure, and various derived quantities measured by Zha *et al.* [4]: anisotropy parameters, sound velocities, Poisson's ratio, etc. We have analyzed these quantities both in the pressure range up to 150 GPa, where experimental data are available and semiempirical potentials are applicable; and in the TPa pressure range (GGA only), where the metallization transition takes place. Both methods (GGA and SE) are in general agreement with the experiment. Most calculated quantities display noticeable features at the metallization point. Zero-point vibrations do not affect the elastic properties of helium in any dramatic way for the pressures considered in the present paper (disregarding the quantum crystal region at very low pressures).

Our calculations predict a significant elastic anisotropy for hcp helium ($\triangle P \approx 1.14$, $\triangle S_1 \approx 1.7$, $\triangle S_2 \approx 0.93$ at low pressures). Both GGA and SE overestimate the anisotropy parameters compared to the experiment, which might be a temperature effect (experiments were carried out at $T = 300$ K). The three anisotropy parameters become more isotropic (close to one) under TPa pressures, with the anisotropy of the shear modes S_1 and S_2 changing sign at the metallization point. Our calculated Poisson's ratio (PR) is in excellent agreement with the $T = 0$, $p = 0$ result of Ref. [26] ($\sigma = 0.38$). Our calculations agree with the experimentally observed [4] decrease of the PR with pressure. Under TPa pressures, PR reaches values ~ 0.31 at the metallization point ($p \approx 17.5$ TPa) and ~ 0.29 at $p = 30$ TPa. We have shown that the negative sign of the pressure dependence of PR is not a quantum effect by performing calculations without zero-point vibrations, which yield similar results.

ACKNOWLEDGMENT

We gratefully acknowledge J. Peter Toennies for valuable discussions.

[1] P. Loubeyre, R. LeToullec, J. P. Pinceaux, H. K. Mao, J. Hu, and R. J. Hemley, Phys. Rev. Lett. **71**, 2272 (1993).
[2] Yu. A. Freiman, S. M. Tretyak, A. Grechnev, A. F. Goncharov, J. S. Tse, D. Errandonea, H.-k. Mao, and R. J. Hemley, Phys. Rev. B **80**, 094112 (2009).
[3] A. Grechnev, S. M. Tretyak, and Yu. A. Freiman, Fizika Nizkikh Temperatur **36**, 423 (2010) [Low. Temp. Phys. **36**, 333 (2010)].
[4] C.-S. Zha, H.-k. Mao, and R. J. Hemley, Phys. Rev. B **70**, 174107 (2004).
[5] K. Takemura, J. Appl. Phys. **89**, 662 (2001).
[6] C.-S. Zha, T. S. Duffy, H.-k. Mao, and R. J. Hemley, Phys. Rev. B **48**, 9246 (1993).
[7] Yu. A. Freiman, A. Grechnev, S. M. Tretyak, A. F. Goncharov, and E. Gregoryanz, Fizika Nizkikh Temperatur **41**, 571 (2015).
[8] Z. Nabi, L. Vitos, B. Johansson, and R. Ahuja, Phys. Rev. B **72**, 172102 (2005).
[9] G. Steinle-Neumann, L. Stixrude, and R. E. Cohen, Phys. Rev. B **60**, 791 (1999).
[10] J. M. McMahon, M. A. Morales, C. Pierleoni, and D. M. Ceperley, Rev. Mod. Phys. **84**, 1607 (2012).
[11] C. Cazorla and J. Boronat, Phys. Rev. B **91**, 024103 (2015).
[12] B. Monserrat, N. D. Drummond, C. J. Pickard, and R. J. Needs, Phys. Rev. Lett. **112**, 055504 (2014).
[13] J. M. Wills, O. Eriksson, P. Andersson, A. Delin, O. Grechnyev, and M. Alouani, *Full-Potential Electronic Structure Method: Energy and Force Calculations with Density Functional and Dynamical Mean Field Theory* (Springer, Berlin, 2010).
[14] J. P. Perdew, K. Burke, and M. Ernzerhof, Phys. Rev. Lett. **77**, 3865 (1996).
[15] Yu. A. Freiman and S. M. Tretyak, Fizika Nizkikh Temperatur **33**, 719 (2007) [Low. Temp. Phys. **33**, 545 (2007)].
[16] Yu. A. Freiman, A. F. Goncharov, S. M. Tretyak, A. Grechnev, J. S. Tse, D. Errandonea, H.-k. Mao, and R. J. Hemley, Phys. Rev. B **78**, 014301 (2008).
[17] Yu. A. Freiman, A. Grechnev, S. M. Tretyak, A. F. Goncharov, C. S. Zha, and R. J. Hemley, Phys. Rev. B **88**, 214501 (2013).
[18] T. H. K. Barron and M. L. Klein, Proc. Phys. Soc. **85**, 523 (1965).
[19] J. P. Watt and L. Peselnick, J. Appl. Phys. **51**, 1525 (1980).
[20] K. Huang, Proc. Roy. Soc. **203**, 178 (1950).
[21] M. J. Mehl, Phys. Rev. B **47**, 2493 (1993).
[22] P. Vinet, J. R. Smith, J. Ferrante, and J. H. Rose, Phys. Rev. B **35**, 1945 (1987).
[23] H. Olijnyk and A. P. Jephcoat, J. Phys.: Condens. Matter **12**, 10423 (2000).
[24] M. J. P. Musgrave, *Crystal Acoustics* (Holden-Day, San Francisco, 1970).
[25] S. A. Khairallah and B. Militzer, Phys. Rev. Lett. **101**, 106407 (2008).
[26] P. Nieto, G. Benedek, and J. P. Toennies, New J. Phys **14**, 013007 (2012).